Structural, electronic, and magnetic properties of vanadium atom-adsorbed $MoSe_2$ monolayer*

Ping Liu(刘萍), Zhen-Zhen Qin(秦真真), Yun-Liang Yue(乐云亮), and Xu Zuo(左旭)†

College of Electronic Information and Optical Engineering, Nankai University, Tianjin 300071, *China*

(Received 5 September 2016; revised manuscript received 6 November 2016; published online 20 December 2016)

Using the first-principles calculations, we study the structural, electronic, and magnetic properties of vanadium adsorbed $MoSe_2$ monolayer, and the magnetic couplings between the V adatoms at different adsorption concentrations. The calculations show that the V atom is chemically adsorbed on the $MoSe_2$ monolayer and prefers the location on the top of an Mo atom surrounded by three nearest-neighbor Se atoms. The interatomic electron transfer from the V to the nearest-neighbor Se results in the polarized covalent bond with weak covalency, associated with the hybridizations of V with Se and Mo. The V adatom induces local impurity states in the middle of the band gap of pristine $MoSe_2$, and the peak of density of states right below the Fermi energy is associated with the V-dz^2 orbital. A single V adatom induces a magnetic moment of 5 μ_B that mainly distributes on the V-3d and Mo-4d orbitals. The V adatom is in high-spin state, and its local magnetic moment is associated with the mid-gap impurity states that are mainly from the V-3d orbitals. In addition, the crystal field squashes a part of the V-4s electrons into the V-3d orbitals, which enhances the local magnetic moment. The magnetic ground states at different adsorption concentrations are calculated by generalized gradient approximations (GGA) and GGA+U with enhanced electron localization. In addition, the exchange integrals between the nearest-neighbor V adatoms at different adsorption concentrations are calculated by fitting the first-principle total energies of ferromagnetic (FM) and antiferromagnetic (AFM) states to the Heisenberg model. The calculations with GGA show that there is a transition from ferromagnetic to antiferromagnetic ground state with increasing the distance between the V adatoms. We propose an exchange mechanism based on the on-site exchange on Mo and the hybridization between Mo and V, to explain the strong ferromagnetic coupling at a short distance between the V adatoms. However, the ferromagnetic exchange mechanism is sensitive to both the increased inter-adatom distance at low concentration and the enhanced electron localization by GGA+U, which leads to antiferromagnetic ground state, where the antiferromagnetic superexchange is dominant.

Keywords: V-adatom, $MoSe_2$ monolayer, magnetic moment, magnetic coupling, first-principles calculation

PACS: 71.15.Mb, 71.20.–b, 73.20.Hb, 75.70.Ak **DOI:** 10.1088/1674-1056/26/2/027103

1. Introduction

Recently, two-dimensional (2D) materials have received a lot of attention because of their potential applications in a wide range of electronic devices, especially in spintronics. In particular, graphene is considered as the most promising candidate for future electronics.[1] However, pristine graphene is metallic without an energy band gap, which may hinder its direct application in semiconducting devices. Layered transition metal dichalcogenides (LTMDs), such as MoS_2, have been discovered to be a new class of 2D materials. Unlike graphene, the LTMDs are semiconducting with a band gap of 1 eV∼2 eV, which makes them promising for low-dimensional semiconducting devices. The LTMDs can be readily prepared by micromechanical exfoliation,[2,3] liquid exfoliation,[4,5] hydrothermal synthesis, and chemical vapor deposition.[1,6] Due to the reduction of dimension, the LTMDs exhibit electronic, mechanical, and optical properties different from their three-dimensional (3D) counterparts, and have received a great deal of theoretical[7,8] and experimental attention.[9,10]

Since pristine $MoSe_2$ monolayer is nonmagnetic, many efforts have been devoted to inducing magnetism. Intrinsic defect, strain, and doping or adsorption of foreign atoms have been proposed to be efficient ways to induce magnetism to LTMDs, and the structural, electronic, and magnetic properties can also be tailored, which make LTMDs promising candidates for spintronic devices. These modifications have been much more extensively investigated for MoS_2[11–14] and WS_2[15–18] monolayers than for $MoSe_2$. Investigations on the modifications of $MoSe_2$ monolayer are limited so far. Ghosh *et al.* found that electronic and optical properties of monolayer $MoSe_2$ can be modulated by equibiaxial strain.[19] Zhang *et al.* studied the effects of vacancy and strain on the magnetic property of monolayer $MoSe_2$.[20] Ma *et al.* explored the vacancy-doped and nonmetal adsorbed $MoSe_2$ monolayer.[17]

In the present work, we select $MoSe_2$ monolayer, a two-dimensional (2D) semiconductor with a direct band gap, as the host material, and study its structural, electronic, and magnetic properties with V adatoms at various adsorption concentrations by using first-principles calculations. The electronic structure calculations show that the V adatom is chem-

*Project supported by the National Basic Research Program of China (Grant No. 2011CB606405), the CAEP Microsystem and THz Science and Technology Foundation, China (Grant No. CAEPMT201501), and the Science Challenge Project, China (Grant No. JCKY2016212A503).

†Corresponding author. E-mail: xzuo@nankai.edu.cn

© 2017 Chinese Physical Society and IOP Publishing Ltd

ically adsorbed on the $MoSe_2$ monolayer, and introduces impurity levels in the middle of the pristine band gap. The magnetic property calculations show that the V adatom induces a magnetic moment in an otherwise nonmagnetic $MoSe_2$ monolayer. Further calculations on the magnetic coupling between the V adatoms show that the magnetic ground state depends on not only the adsorption concentration but also the on-site Coulomb repulsion of the V-3d orbitals. The calculations with generalized gradient approximation (GGA) show a transition from ferromagnetic (FM) to antiferromagnetic (AFM) ground state, while the GGA+U calculations lead to AFM ground state for all investigated concentrations. We propose a ferromagnetic exchange mechanism involving the on-site exchange of Mo and the hybridization between Mo and V, to explain the FM coupling at a short distance between the V adatoms. Both the increased inter-adatom distance at low concentrations and the enhanced electron localization by GGA+U weaken the FM exchange mechanism, and lead to AFM ground state, where the AFM superexchange is dominant and in agreement with the value estimated from the calculated density of states (DOS).

2. Computational methods

The first-principles calculations are based on density functional theory (DFT), and implemented by the Vienna *ab initio* simulation package (VASP).[21] The exchange and correlation are treated by the Perdew–Burke–Ernzerhof (PBE) parameterization of GGA.[22] The projector augmented plane-wave (PAW) method is adopted to describe the electron–ion interaction,[23] and the plane-wave cutoff energy is set to be 450 eV. A vacuum layer of 15 Å in thickness is used to isolate the interaction between the $MoSe_2$ sheet and its periodic images along the z-axis. The atomic structures of 2×2, 3×3, and 4×4 supercells are optimized by using conjugate gradient algorithm with a $7\times7\times1$ Monkhorst–Pack k-mesh for the first two and with a $3\times3\times1$ k-mesh for the last one, until the residual force on each atom is less than 0.02 eV/Å and the total energy difference between two consecutive ionic steps is less than 10^{-5} eV. After the structural optimization, the electronic and magnetic properties are calculated with a denser k-mesh of $7\times7\times1$ and a higher accuracy of total energy of 10^{-6} eV for all supercells. In addition to the GGA calculations, the electronic structure and magnetic properties are calculated by using GGA+U (GGA plus on-site Coulomb repulsion),[24] where the U parameter is chosen to be 3.0 eV for the V-3d orbitals.[25] The magnetic couplings at different adsorption concentrations are calculated by using both GGA and GGA+U approaches. The valence electron configurations are $4s^24p^4$, $4d^55s^1$, and $3d^34s^2$ for Se, Mo, and V, respectively.

3. Results and discussion

3.1. Atomic structure

$MoSe_2$ monolayer is comprised of the Se, Mo, and Se atom layers stacked along the z axis, where the Mo layer is sandwiched between two layers of Se. The $MoSe_2$ monolayer belongs to space group $P\bar{6}m2$, and a Mo atom is locally coordinated by six nearest-neighbor Se atoms forming a trigonal prism. The structure is identical to other LTMDs, such as MoS_2. The perfect 4×4 $MoSe_2$ supercell is plotted in Figs. 1(a) and 1(b). After the structural optimization, the lattice constant of pristine $MoSe_2$ monolayer is 3.319 Å. The Mo–Se bond length and Se–Mo–Se bond angle are 2.541 Å and 82.10°, respectively, which are in good agreement with previous calculations.[26]

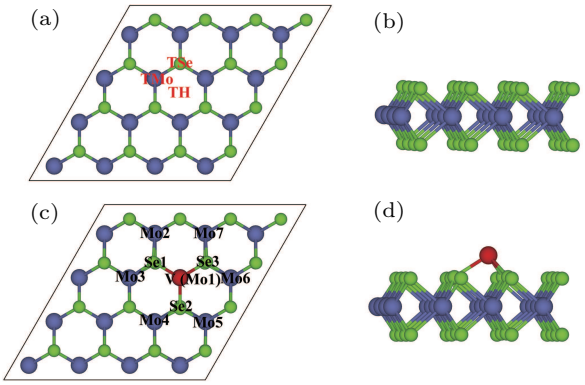


Fig. 1. (color online) (a) Top and (b) side views of pristine 4×4 $MoSe_2$ monolayer unit cell, (c) top and (d) side views of the stablest TMo configuration by structural optimization. Three adsorption sites, namely TMo, TSe, and TH are labeled in panel (a). The green, grey, and red balls represent Se, Mo, and V atoms, respectively.

For the V atom adsorbed $MoSe_2$ sheet, three possible high-symmetry positions have been considered as shown in Fig. 1(a). A vanadium atom is placed at the TMo, TSe, or TH site, where the TMo, TSe, and TH denote the tops of Mo, Se, and center of hexagons projected on *ab* plane, respectively. The adsorption energy (E_{ad}) is defined as follows:

$$E_{ad} = E_{tot} - E_{mono} - E_{atom}, \tag{1}$$

where E_{tot}, E_{mono}, and E_{atom} are the total energies of an adsorption configuration, pristine $MoSe_2$ monolayer, and a free V atom, respectively. Figure 2 depicts the adsorption energies of V atom at three adsorption sites, which indicates that V adatom is chemically adsorbed on $MoSe_2$ monolayer with site-dependent adsorption energy. It is obvious that the stablest configuration is the TMo site, which is consistent with that of V-adsorbed MoS_2 monolayer.[27] In addition, the calculated adsorption energy for the TMo site is −3.90 eV, which is 0.61 eV and 1.07 eV lower than those of TH and TSe sites, respectively. The large adsorption energy and migration barriers guarantee the thermal stability of the V atom adsorbed on the TMo site.

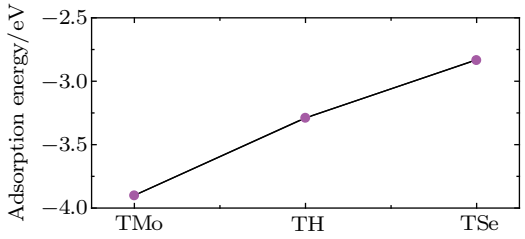


Fig. 2. (color online) Adsorption energies of V adatom at the three sites on 4×4 $MoSe_2$ monolayer.

To examine the influence of V adatom on the structure of $MoSe_2$ monolayer, the structural relaxation induced by the V adsorption is measured. Table 1 summarizes the structure parameters of the stablest configuration. The height of the V adatom (h_V) is estimated by the distance from the V atom to the plane determined by the three nearest-neighbor Se atoms, and the corrugation of $MoSe_2$ monolayer (C_M) is measured by calculating the difference between the maximum and minimum z-coordinates of the upper Se layer. For the stablest adsorption configuration, the optimized structures of the V-adsorbed $MoSe_2$ monolayer are drawn in Figs. 1(c) and 1(d), where a slight local distortion appears near the V adatom. In the pristine $MoSe_2$ monolayer, the distances between the Mo atom and the six nearest-neighbor Se atoms are equal. However, for the V-adsorbed system, the three adjacent Se atoms in the upper layer move away from the Mo atom and the Mo–Se bonds are elongated by 0.094 Å to 2.635 Å. At the same time, the other three Mo–Se bonds are slightly shrunk to 2.538 Å.

Table 1. Calculated structure parameters of the $MoSe_2$ monolayer with a V adatom: the stablest adsorption site (site), adsorption energy (E_{ad}), distance between the V adatom and the nearest neighbor Mo atom (d_{V-Mo}), distance between the V adatom and the nearest neighbor Se atom (d_{V-Se}), corrugation (C_M), adsorption height (h_V), and total magnetic moment (M_{tot}).

Site	E_{ad}/eV	d_{V-Mo}/Å	d_{V-Se}/Å	C_M/Å	h_V/Å	M_{tot}/μ_B
TMo	–3.90	2.962	2.418	0.093	1.296	5

The distortion is attributed to the covalent bond between the V adatom and the three nearest-neighbor Se atoms, associated with the charge transfer from the V to the Se atoms. The charge density difference is illustrated in Fig. 3, defined by

$$\Delta\rho = \rho_{tot} - \rho_{mono} - \rho_{atom}, \tag{2}$$

where ρ_{tot} is the charge density of the $MoSe_2$ monolayer with the V adatom, and ρ_{mono} and ρ_{atom} are the charge densities of the pristine $MoSe_2$ monolayer and the free V atom, respectively. The calculated results reveal that there exists a distinct charge transfer between the V adatom and the $MoSe_2$ sheet, which results in the V–Se covalent bond (Fig. 3). The Bader charge analysis[28,29] shows that the three Se atoms near the V adatom are negatively charged and each of them accommodates about 0.606 electron, and that the V adatom loses 0.791 electron and is positively charged (Table 2). Therefore, the positively charged V atom pulls the three neighboring Se atoms, which leads to the corrugation of the $MoSe_2$ sheet.

Table 2. Values of local magnetic moment (M) and the charge transfer (Q). The positive (negative) Q values represent accepting (losing) electrons. NN represents the nearest neighbor of the V atom. 2nd NN and 3rd NN represent the second- and third-nearest-neighbor of the V atom.

	2nd NN			3rd NN					NN		
	V	Mo	(Mo_2	Mo_3	Mo_4	Mo_5	Mo_6	Mo_7)	(Se_1	Se_2	Se_3)
M/μ_B	3.331	0.377	0.113	0.112	0.111	0.110	0.111	0.112	–0.014	–0.014	–0.014
Q/e	–0.791	-0.788	–0.798	–0.794	–0.794	–0.798	–0.838	–0.838	0.606	0.606	0.607

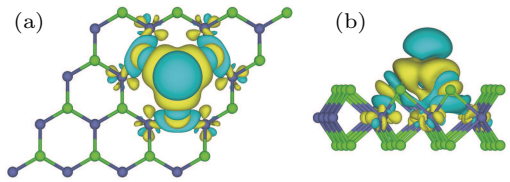


Fig. 3. (color online) (a) Top view and (b) side view of the isosurface (at ± 0.001 e/Å^3) of charge density difference of the $MoSe_2$ monolayer with a V adatom. Yellow and cyan colors represent positive and negative charge densities, respectively

3.2. Electronic structure

The electronic band structure, and the total and projected density of states (TDOS and PDOS) of the pristine 4×4 $MoSe_2$ monolayer are plotted in Fig. 4, and those of the $MoSe_2$ monolayer with the V adatom in Fig. 5. It is evident that the pristine $MoSe_2$ monolayer is a semiconductor with a direct band gap of 1.47 eV at K point [Fig. 4(a)], which is in good agreement with previous theoretical[26] and experimental results.[30] In Fig. 4(b), the majority and minority spins are symmetric, which implies that the pristine $MoSe_2$ monolayer may be nonmagnetic. The valence band maximum (VBM) and conduction band minimum (CBM) are primarily from the Mo-4d states. The hybridization between Mo-4d and Se-4p states is associated with the weak covalency between Mo and Se atoms [Figs. 4(c) and 4(d)].

The adsorption of V atom induces magnetism, and the majority and minority spins become asymmetric [Figs. 5(a) and 5(b)]. The adsorption induces almost flat impurity levels only in the middle of majority band gap, at -0.928, -0.413, and -0.006 eV below the Fermi energy, respectively. These narrow impurity states primarily arise from the V-3d states with hybridization of the Se-4p and Mo-4d (Figs. 5(c)–5(e)). Projected DOS show that the DOS peak at the Fermi energy is mainly from the dz^2 orbital of V adatom (Figs. 5(e) and 5(f)). Moreover, from Figs. 5(c) and 5(d), the Mo and Se atoms are also slightly spin-polarized due to hybridization with the V adatom.

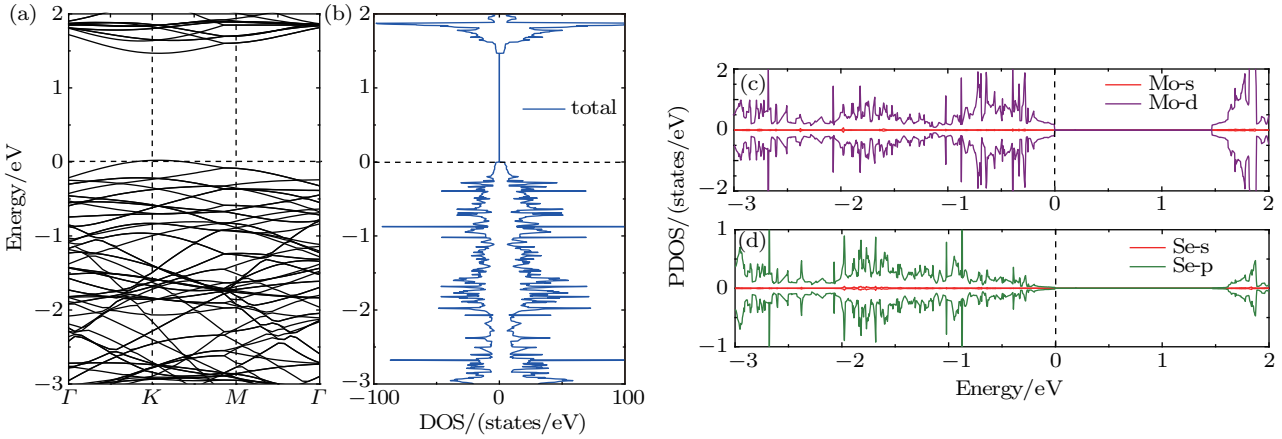


Fig. 4. (color online) Electronic band structure (a), total DOS (b), and DOS projected on Mo (c) and Se (d) of pristine 4×4 $MoSe_2$ monolayer. The Fermi level is aligned to zero.

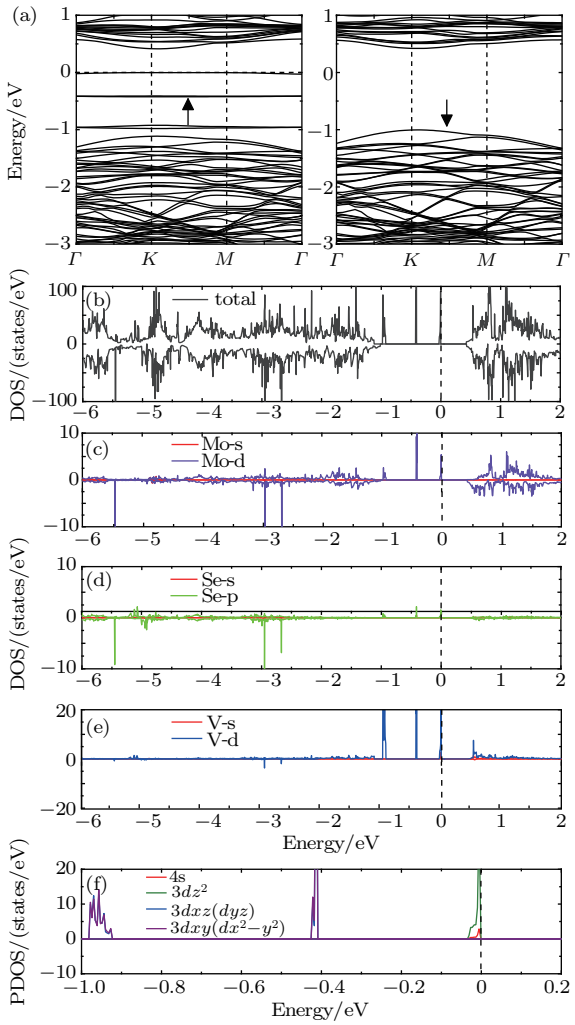


Fig. 5. (color online) Spin-polarized band structures (a), where up (down) arrow indicates majority (minority) spin, the total DOS (b), and PDOS ((c)–(e)) of 4×4 $MoSe_2$ monolayer with the V adatom. DOS is projected onto the V adatom (e), and its nearest-neighbor Mo (c) and Se (d) atoms. The details of panel (e) around the Fermi energy are shown in panel (f). The Fermi energy is aligned to zero.

3.3. Magnetic moments

Integrating the total DOS over the whole energy range results in 149 majority and 144 minority spins. A single V adatom with 5 valence electrons thus induces 5 μ_B net magnetic moment, approximately equal to that induced for an MoS_2 monolayer.[27] The induced magnetic moment is associated with the mid-gap impurity states of majority spin, where two of them (d_{xy} and $d_{x^2-y^2}$, and d_{xz} and d_{yz}) are doublet and one (d_{z^2}) is singlet. The 5 valence electrons of the V adatom all fill in the mid-gap impurity states and induce a total magnetic moment of 5 μ_B.

The local magnetic moment on the V adatom inside the muffin-tin radius is 3.331 μ_B, a major contribution to the total magnetic moment. The local magnetic moment on the Mo atom right below the V adatom is 0.377 μ_B, and that of the six third-nearest neighbor Mo atoms in total is 0.669 μ_B (Table 2).

In order to observe the detailed distribution of magnetic moment, we depict spin density isosurface in Fig. 6. It is obvious that the spin density is mainly localized around the V adatom, and the six third-nearest-neighbor Mo atoms, each of which shows a positive spin density. However, the nearest-neighbor Se atom shows a negative spin density.

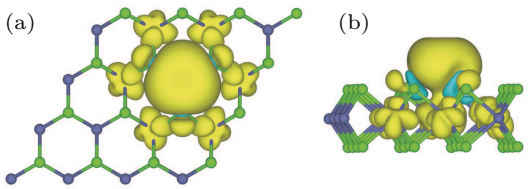


Fig. 6. (color online) Isosurfaces at spin density 0.001 e/Å^3 of V-adsorbed $MoSe_2$ monolayer in top (a) and side (b) views. Yellow and cyan colors represent majority and minority spin densities.

In addition, compared with the ideal value of 3 μ_B of a free V atom, the local magnetic moment of V adatom is slightly increased by 0.331 μ_B, which is attributed to the inter-orbital charge transfer. Compared with that contributed by the free V atom configuration ($3d^3 4s^2$), the magnetic moments contributed by the 4s and 3d orbitals are 0.069 and 3.223 μ_B for the V adatom.

Under the C_{3V} local symmetry from the Se trigonal prism, the five 3d orbitals of V adatom will split into a singlet d_{z^2} with A_1 symmetry, and two doublets (d_{xz}, d_{yz}) and ($d_{x^2-y^2}$, d_{xy})

both with E symmetry. In addition, V-4s orbital also has the A_1 symmetry. The orbitals with compatible symmetry will hybridize with each other and further with the dangling bonds of the nearest-neighbor Se atoms, which results in the V group of molecular orbitals, a singlet with A_1 symmetry and two doublets both with E symmetry, with the energies ranging from high to low as indicated by $1A_1$, $1E$, and $2E$ in Fig. 7, which correspond to the mid-gap defect states [Figs. 5(a) and 5(f)]. As a result, part of the s-electrons transfer to the d_{z^2} orbital in the V adatom. In addition, it is obvious from Fig. 5(a) that the V adatom is in high spin state, and the s-to-d electron transfer increases the number of unpaired d-electrons. This results in an increase of the local magnetic moment on the V adatom, as in the V-adsorbed BN[31] and MoS_2 monolayers.[27]

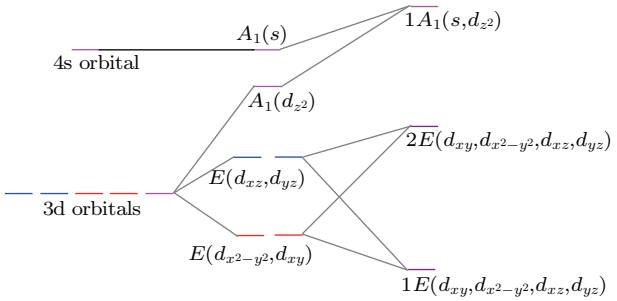


Fig. 7. (color online) Schematic diagram of molecular orbitals of the V adatom, where the left part shows the orbitals of a free V atom, the middle part refers to those orbitals in C_{3v} local symmetry, and the right part denotes the molecular orbitals corresponding to the mid-gap states in Figs. 5(a) and 5(f). Note only the molecular orbitals of V-group are shown here.

3.4. Magnetic coupling

We investigate the magnetic ground state and magnetic coupling between the nearest-neighbor V adatoms. The 2×2, 3×3, and 4×4 supercells are doubled along one edge in the ab plane into 4×2, 6×3, and 8×4, respectively, to investigate the influence of adsorption concentration on magnetic ground state.[32,33] The energy differences between the AFM and the FM states, $\Delta E = E_{\rm AFM} - E_{\rm FM}$, are calculated and listed in Table 3. If the difference is positive (negative), the FM (AFM) state is stabler. In addition, the exchange integrals are calculated by fitting the first-principles energies of FM and AFM states into the nearest-neighbor Heisenberg Hamiltonian,

$$H = -J\sum_{\langle i,j\rangle} \boldsymbol{S}_i \cdot \boldsymbol{S}_j, \tag{3}$$

where J is the exchange integral, $\boldsymbol{S}_i$ and $\boldsymbol{S}_j$ are the spins taking value of 3/2, the nominal value of V^{2+}, and $\langle i,j\rangle$ is the summation over the nearest-neighbor V pairs. The positive (negative) J indicates an FM (AFM) magnetic coupling between the nearest-neighbor V adatoms.[34] The calculated results are listed in Table 3, from which it is obvious that the magnetic coupling depends on not only the distance between the adatoms but also the on-site Coulomb repulsion.

The results calculated with GGA indicate that the sign of the magnetic coupling changes from positive to negative value with increasing V–V distance. When the V–V distance is 6.639 Å, corresponding to an adsorption concentration of 1/12, the magnetic coupling between the two adatoms is FM, and the local magnetizations on the two nearest-neighbor adatoms tend to be parallel to each other. However, when the V–V distance increases to 9.958 Å, the magnetic coupling flips its sign and the magnetic ground state becomes AFM. This result is in qualitative agreement with the results in BN monolayer decorated with foreign atoms[35] and other 2D diluted magnetic systems.[36] However, GGA+U calculations lead to AFM magnetic ground states and couplings at all distances. It also induces a monotonic and faster damping of the magnetic coupling, of which the magnitude decreases from 42.0 meV at 6.639 Å to 0 at 13.278 Å. This is also found in other diluted magnetic insulators, such as V-doped anatase TiO_2.[25]

For a better understanding of the magnetic coupling, we calculate the DOSs of the magnetic ground states of the 4×2 and 6×3 supercells by GGA and GGA+U [Figs. 8(c)–8(f)], where the magnetic ground state of 4×2 supercell by GGA is FM and all others are AFM.[37,38] The magnetic ground states reflect the competing FM and AFM exchange mechanisms.[39,40] Since all magnetic ground states are insulating, the exchange mechanisms requiring a metallic state, such as double exchange and RKKY interaction, are excluded. More than that, only the ground state of the 4×2 supercell by GGA (Table 3) is FM, which hints that the FM exchange mechanism dominant in this system may be more sensitive to the inter-adatom distance and on-site Coulomb repulsion.[41]

In fact, a strong FM exchange mechanism in the 4×2 supercell by GGA is associated with the Mo atom shared by two nearest-neighbor V adatoms as a 3rd nearest neighbor. From the isosurface of spin density (Fig. 6), it is obvious that the V adatom induces spin polarization with respect to its 3rd nearest neighbor Mo atoms, and the spin distributions of the two Mo atoms on a diagonal of the Mo hexagonal are approximately orthogonal to each other. Therefore, two nearest-neighbor V atoms in the 4×2 supercell respectively induce spin polarizations with respect to two (approximately) orthogonal orbitals in the shared Mo atom, and the on-site exchange of Mo tends to align the spin distributions respectively induced by the two V adatoms parallel to each other according to Hund's rule.

The strength of the above FM exchange can be estimated on the assumption that the on-site exchange energy follows the Dudarev formulation,

$$E_{\rm ex} \approx -\frac{1}{2} I \sum_{m,\sigma} \left(n_{m,\sigma} - n_{m,\sigma}^2\right), \tag{4}$$

where $n_{m\sigma}$ is the population of the m-th d-orbital with spin σ, and I is the on-site exchange parameter. Considering only

the two orbitals with induced spin polarization, we obtain $n_{m\sigma} \sim 0.05$ from the total magnetic moment of ~ 0.1 μ_B and ignore the square term in Eq. (4). Thus, the on-site exchange energy can be related to the total magnetic moment in Bohr magneton, m, by

$$E_{ex} \approx -\frac{1}{2} Im. \tag{5}$$

Since two nearest-neighbor V adatoms share a 3rd nearest-neighbor Mo atom and each V adatom has 6 nearest neighbors in the lattice shown in Fig. 8(a), the exchange energy of the Mo atom leads to a positive contribution to the energy difference between AFM and FM states per V atom,

$$\Delta E' \approx \frac{3}{2} Im. \tag{6}$$

Using the typical value of on-site exchange for 4d atoms, $I \sim 0.2$ eV, and the total magnetic moment on Mo given by Table 2, $m \sim 0.1$ μ_B, we estimate that $\Delta E' \sim 30$ meV per V atom, or ~ 60 meV per 4×2 unit cell, corresponding to an FM exchange integral of $J' \sim 13$ meV. However, it should be noted that the atomic value of on-site exchange, I, may be renormalized by the hybridization between Mo and 3d atoms, and the resulting effective value, I_{eff}, can be enhanced up to ~ 1 eV.[41]

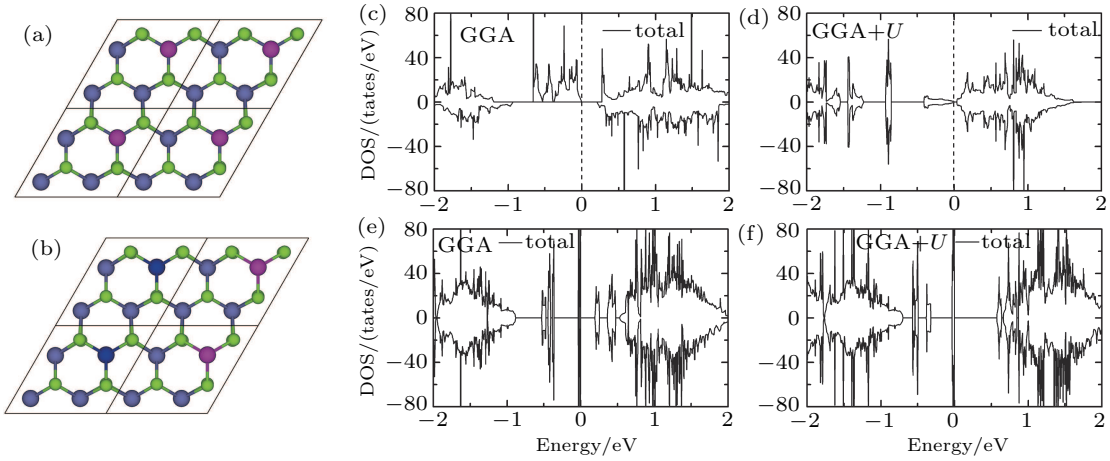


Fig. 8. (color online) Illustrations of the FM (a) and AFM (b) structures for V-adsorbed $MoSe_2$ monolayer at the a concentration of 1/12, where the red and blue balls represent the spin-up and spin-down V adatoms, respectively, and the green and gray balls represent Se and Mo atoms, respectively. The total DOSs of 4×2 supercell by GGA (c) and GGA+U (d), and those of 6×3 supercell by GGA (e) and GGA+U (f), where the magnetic ground state of 4×2 supercell by GGA is FM and others are AFM.

It is obvious that the above FM exchange mechanism is sensitive to both inter-adatom distance and on-site Coulomb repulsion. When the inter-adatom distance is increased, two nearest-neighbor V adatoms will no longer share a 3rd nearest-neighbor Mo atom, and thus the FM exchange mechanism will vanish. When extra on-site Coulomb repulsion is applied to V-d orbitals by GGA+U approach, the enhanced on-site Coulomb repulsion will significantly reduce the Mo–V hybridization and thus the total magnetic moment is shared by Mo atoms, which results in a much smaller $\Delta E'$.

When the inter-adatom distance increases or extra on-site Coulomb repulsion is applied, the dominant exchange mechanism will be the AFM superexchange,[42]

$$J_2 = -\frac{4|t_{V-V}|^2}{U_{eff}}, \tag{7}$$

where t_{V-V} is the effective hopping between two nearest neighbor V adatoms, and U_{eff} is the effective on-site Coulomb repulsion of V adatom. The t_{V-V} can be estimated by using the approximation $w \sim zt_{V-V}$, where w is the bandwidth of V impurity band, and $z = 6$ is the number of nearest neighbors. Both w and U_{eff} can be directly read out from the DOS. The values of AFM superexchange, J_2, estimated from the DOS are listed in Table 3.

Table 3. Energy differences between the AFM and FM states, $\Delta E = E_{AFM} - E_{FM}$, for the V-adsorbed $MoSe_2$ monolayer by GGA and GGA+U approaches at different adsorption concentrations. The d_{V-V} is the distance between the V atoms, J is the exchange interaction calculated from ΔE, w, and U_{eff} are the bandwidth of V impurity band and the effective on-site Coulomb repulsion from DOS, J_2 is the AFM superexchange estimated from Eq. (7). The values in the parentheses are calculated by using GGA+U approach.

Concentration	1/12	1/27	1/48
d_{V-V}/Å	6.639	9.958	13.278
ΔE/meV	14.2 (–42.0)	–11.2 (–3.61)	–0.25 (0)
J/meV	3.16 (–9.33)	–2.49 (–0.80)	0 (0)
w/meV	300 (200)	60 (40)	N/A
U_{eff}/meV	0.2 (0.6)	0.2 (0.6)	N/A
J_2/meV	–50 (–7.4)	-2 (–0.3)	N/A

4. Conclusions

In this study, we carry out the first-principles calculations to investigate the structural, electronic, and magnetic characteristics of V-adsorbed $MoSe_2$ monolayer. The calculations indicate that the most favorable adsorption site is on the top of a Mo atom, and that the V adatom can induce impurity states

in the middle of the band gap, which are mainly from the V-3d states with hybridization of the Mo-4d and Se-4p states. The V adatom induces magnetism for the $MoSe_2$ monolayer, which is associated with the mid-gap impurity states of majority spin. Further, the inter-orbit electron transfer from V-s to V-d slightly enhances the local magnetic moment on the V adatom. The magnetic ground state depends on not only the adsorption concentration but also the on-site Coulomb repulsion. A ferromagnetic exchange mechanism is proposed to explain the FM ground state given by GGA calculations at a high adsorption concentration of 1/12, based on the on-site exchange of Mo and the hybridization between Mo and V. The AFM superexchanges are also estimated by using the parameters extracted from the calculated DOS.

References

[1] Song X F, Hu J L and Zeng H B 2013 *J. Mater. Chem. C* **1** 2952
[2] Zhang Y J, Ye J T, Matsuhashi Y and Iwasa Y 2012 *Nano Lett.* **12** 1136
[3] Radisavljevic B, Radenovic A, Brivio J, Giacometti V and Kis A 2011 *Nat. Nanotechnol.* **6** 147
[4] Coleman J N, Lotya M, O'Neill A, *et al*. 2011 *Science* **331** 568
[5] Nicolosi V, Chhowalla M, Kanatzidis M G, Strano M S and Coleman J N 2013 *Science* **340** 1226419
[6] Lee Y H, Zhang X Q, Zhang W J, Chang M T, Lin C T, Chang K D, Yu Y C, Wang J T W, Chang C S, Li L J and Lin T W 2012 *Adv. Mater.* **24** 2320
[7] Lei T M, Wu S B, Zhang Y M, Liu J J, Guo H and Zhang Z Y 2013 *Rare Met. Mater. Eng.* **42** 2477
[8] Huang W, Luo X, Gan C K, Quek S Y and Liang G C 2014 *Phys. Chem. Chem. Phys.* **16** 10866
[9] Mak K F, He K L, Lee C, Lee G H, Hone J, Heinz T F and Shan J 2013 *Nat. Mater.* **12** 207
[10] Jones A M, Yu H Y, Ghimire N J, Wu S F, Aivazian G, Ross J S, Zhao B, Yan J Q, Mandrus D G, Xiao D, Yao W and Xu X D 2013 *Nat. Nanotechnol.* **8** 634
[11] Chen Z P, He J J, Zhou P, Na J and Sun L Z 2015 *Comput. Mater. Sci.* **110** 102
[12] Cao J, Cui L and Pan J 2013 *Acta Phys. Sin.* **62** 187102 (in Chinese)
[13] Andriotis A N and Menon M 2014 *Phys. Rev. B* **90** 125304
[14] Wu M S, Xu B, Liu G and Quyang C Y 2013 *Acta Phys. Sin.* **62** 037103 (in Chinese)
[15] Shi H L, Pan H, Zhang Y W and Yakobson B I 2013 *Phys. Rev. B* **87** 155304
[16] Zhao X, Dai X Q, Xia C X, Wang T X and Peng Y T 2015 *Solid State Commun.* **215** 1
[17] Ma Y D, Dai Y, Guo M, Niu C W, Lu J B and Huang B B 2011 *Phys. Chem. Chem. Phys.* **13** 15546
[18] Zhao X, Xia C X, Wang T X, Peng Y T and Dai X Q 2015 *J. Alloys Compd.* **649** 357
[19] Ghosh C K, Sarkar D, Mitra M K and Chattopadhyay K K 2013 *J. Phys. Appl. Phys.* **46** 395304
[20] Zhang H, Fan X L, Yang Y and Xiao P 2015 *J. Alloys Compd.* **635** 307
[21] Kresse G and Furthmüller J 1996 *Comput. Mater. Sci.* **6** 15
[22] Perdew J P, Burke K and Ernzerhof M 1996 *Phys. Rev. Lett.* **77** 3865
[23] Blöchl P E 1994 *Phys. Rev. B* **50** 17953
[24] Dudarev S L, Botton G A, Savrasov S Y, Humphreys C J and Sutton A P 1998 *Phys. Rev. B* **57** 1505
[25] Du X S, Li Q X, Su H B and Yang J L 2006 *Phys. Rev. B* **74** 233201
[26] Mishra R, Zhou W, Pennycook S J, Pantelides S T and Idrobo J C 2013 *Phys. Rev. B* **88** 144409
[27] Wang Y Z, Wang B L, Huang R, Gao B L, Kong F J and Zhang Q F 2014 *Phys. E Low-Dimens. Syst. Nanostructure* **63** 276
[28] Henkelman G, Arnaldsson A and Jónsson H 2006 *Comput. Mater. Sci.* **36** 354
[29] Bader R F W 1985 *Acc. Chem. Res.* **18** 9
[30] Tongay S, Zhou J, Ataca C, Lo K, Matthews T S, Li J B, Grossman J C, and Wu J Q 2012 *Nano Lett.* **12** 5576
[31] Li J, Hu M L, Yu Z Z, Zhong J X and Sun L Z 2012 *Chem. Phys. Lett.* **532** 40
[32] Li C D, Zhao J L, Zhong C G, Dong Z C and Fang J H 2014 *Acta Phys. Sin.* **63** 087502 (in Chinese)
[33] Li N N, Li H, Tang R L, Han D D, Zhao Y S, Gao W, Zhu P W and Wang X 2014 *Chin. Phys. B* **23** 046105
[34] Masrour R, Hamedoun M, Benyoussef A, Hlil E K, Mounkachi O and Moussaoui H E 2014 *Chin. Phys. Lett.* **31** 037501
[35] Ataca C and Ciraci S 2010 *Phys. Rev. B* **82** 165402
[36] Power S R and Ferreira M S 2013 *Crystals* **3** 49
[37] Hu F, Zhang G Y, Yang D, Zhang X L, Xue L P and Zhang L 2013 *Chin. Phys. Lett.* **30** 087803
[38] Zheng Y L, Lu M C, Guo H X and Bao X L 2015 *Acta Phys. Sin.* **64** 177501 (in Chinese)
[39] Cui Y, Li Y R, Li R Y and Wang Y P 2014 *Chin. Phys. B* **23** 067504
[40] Zheng Y L, Wang X X, Ge Z L, Guo H L, Yan G F, Dai S H, Zhu X L and Tian X B 2013 *Acta Phys. Sin.* **62** 227701 (in Chinese)
[41] Sarma D D, Mahadevan P, Saha-Dasgupta T, Ray S and Kumar A 2000 *Phys. Rev. Lett.* **85** 2549
[42] Tian Y, Shen S P, Cong J Z, Yan L Q, Chai Y S and Sun Y 2016 *Chin. Phys. B* **25** 017601